EQ10060

Algorithms for the Computation of Solutions of the Ornstein–Zernike Equation

A. T. Peplow

Department of Mathematics, Imperial College,

180 Queen's Gate, South Kensington,

London, SW7 2AZ.; a.peplow@ic.ac.uk.

R. E. Beardmore

Department of Mathematics, Imperial College,

180 Queen's Gate, South Kensington,

London, SW7 2AZ; r.beardmore@ic.ac.uk

F. Bresme

Department of Chemistry, Imperial College,

South Kensington, London, SW7 2AZ; f.bresme@ic.ac.uk

Abstract

We introduce a robust and efficient methodology to solve the Ornstein-Zernike integral equation using the pseudo-arc length (PAL) continuation method that reformulates the integral equation in an equivalent but non-standard form. This enables the computation of solutions in regions where the compressibility experiences large changes or where the existence of multiple solutions and so-called branch points prevents Newton's method from converging. We illustrate the use of the algorithm with a difficult problem that arises in the numerical solution of integral equations, namely the evaluation of the so-called *no-solution line* of the Ornstein-Zernike Hypernetted Chain (HNC) integral equation for the Lennard-Jones potential. We are able to use the PAL algorithm to solve the integral equation along this line and to connect physical and non-physical solution branches (both isotherms and isochores) where appropriate.

We also show that PAL continuation can compute solutions within the *no-solution region* that cannot be computed when Newton and Picard methods are applied directly to the integral equation. While many solutions that we find are new, some correspond to states with negative compressibility and consequently are not physical.

We would like to invite the interested reader to send an email to REB in order to obtain a copy of the Matlab files used in this study.

I. INTRODUCTION

The Ornstein-Zernike (OZ) relation represents a powerful approach to investigating the structure and thermodynamics of condensed phases [9]. Different closures must be augmented with the OZ relation in order to obtain a problem that is soluble and for the case of the hypernetted chain (HNC) closure it has been noted that the resulting equation exhibits a forbidden region where no physical real solutions are found for certain density and temperature conditions [2, 3, 13, 14, 18].

This so called *no-solution region* has been taken as an approximation to the liquid-vapour coexistence curve in the past, although it has also been noted in the cited numerical studies that it does not always appear to be connected to a divergence of isothermal compressibility, as should be observed when approaching a coexistence region.

The divergence of the isothermal compressibility that defines the spinodal line *is* observed in some integral equations, such as the MSA [5]. In this particular instance, it has been pointed out that the numerical solution of the integral equation can differ from the analytical result unless the numerical solution is obtained with great care, see also [4]. Even more dramatically, an integral equation that bears a formal resemblance to OZ-HNC has been constructed in [16] in such a way that there is absolutely no correspondance between the solutions of the integral equation and the solutions of its discretisation. This may be a problem when solving integral equations such as OZ-HNC and when using interatomic potentials such as the Lennard-Jones, since these theories can only be solved using a numerical approach.

We should like to point out there are three issues regarding the accurate computation of solutions of any nonlinear integral equation: (1) how that equation is discretised, (2) how that discretisation is solved subject to a suit-

(August 2, 2006)

ably small error tolerance and (3) how well the numerically computed solutions actually approximate a true solution of the underlying equation. This paper only concerns problem (2) from this list, although our discretisation method from step (1) is a slight improvement on the standard one in that convolutions are computed in a manner that is equivalent to replacing the trapezium rule with Simpson's rule. Problem (3) is a problem in theoretical numerical analysis that is not addressed here at all.

Our *numerically-obtained* solutions of the OZ-HNC integral equation suggest that the *no-solution line* results from the divergence of two square root branch points and the subsequent existence of multiple solutions [2]. In [1] it is argued that the existence of this behaviour in the numerical realisation of the OZ-HNC equation is logically consistent with the existence of a true spinodal in the OZ-HNC equations. Another study [13] argues that the *no-solution region* is connected to the onset of complex solutions, although this property is simply a consequence of the existence of branch points.

In this article we discuss a very general methodology that has existed for over thirty years in the numerical mathematics literature [10] and apply it to the Ornstein-Zernike equation. We illustrate its use with the HNC closure, but we would like to emphasise that the method is completely general and can be used with other closures too. One of our aims is to develop a method that is robust in the vicinity of the no-solution line and in regions where compressibility exhibits large changes, including divergence due to the existence of a critical region.

There are a number of algorithms that are suitable for such 'bifurcation problems'. One of these is the pseudo-arc length (PAL) continuation method and we show that the implementation of this method and the reformulation of the HNC integral equation in a non-standard manner results in an efficient methodology that can be easily employed to investigate the no-solution line. This method resolves many of the deficiencies associated with Newton and Picard methods and enables one to find solutions that cannot be found using the latter methods directly.

The structure of the paper is as follows. First we introduce the problem and briefly discuss the origin of the limitations of the traditional Newton method when applied to problems with branch points. There follows a discussion of the numerical implementation of the arc-length continuation method and we then present our results for the OZ-HNC integral equation using the Lennard-Jones potential, our conclusions close the paper.

II. THE ORNSTEIN-ZERNIKE EQUATIONS, NEWTON'S ALGORITHM AND BIFURCATIONS

The Ornstein–Zernike (OZ) equation with hypernetted chain (HNC) closure is the following problem: find functions h and c such that

$$h(r) - c(r) = \rho \int_{\mathbb{R}^3} h(\|x - y\|)c(\|y\|)dy, \tag{1}$$

$$h(r) = -1 + e^{-\beta u(r)} \cdot e^{h(r)-c(r)}. \tag{2}$$

Here x and y are vectors in three-dimensional space, $r = \|x\|$ is the radial coordinate where $\|(x_1, x_2, x_3)\| = (x_1^2 + x_2^2 + x_3^2)^{1/2}$ is Euclidean distance, ρ is the mean particle density, $\beta = 1/(k_B T)$ is the Boltzmann factor, T the temperature and $u(r)$ is the intermolecular potential. The total (h) and direct (c) correlation functions yield the indirect correlation function $\gamma = h - c$ and, using this definition, equations (1-2) can be re-written as a single integral equation of the form

$$\gamma = \rho(f + e^{-\beta u}(\exp \gamma - 1)) * (f + e^{-\beta u}(\exp \gamma - 1) - \gamma), \tag{3}$$

where $f(r) = -1 + e^{-\beta u(r)}$ is the Mayer f-function and $*$ denotes convolution.

Isothermal compressibility κ_T is defined by

$$\kappa_T = \left((\rho k_B T)(1 - 4\pi\rho \int_0^\infty r^2 c(r)dr) \right)^{-1}, \tag{4}$$

the value of which is obtained numerically by evaluating $\int_0^R r^2 c(r)dr$ for a *large* value of R and when plotting the results of computations we shall use

5   (August 2, 2006)

the normalised inverse compressibility χ^{-1}, where

$$\chi = \frac{1}{1 - 4\pi\rho \int_0^\infty r^2 c(r) dr} = 1 + 4\pi\rho \int_0^\infty r^2 h(r) dr. \qquad (5)$$

The OZ-HNC equation may therefore be written as a single equation of the form

$$\gamma = \rho N(\gamma, \beta), \qquad (6)$$

where N is a suitably-defined nonlinear function, which is convenient for the presentation of numerical algorithms. For instance the Picard method is given by

$$\gamma_{n+1} = \rho N(\gamma_n, \beta), \qquad \gamma_0 \text{ an initial guess}, \qquad (7)$$

and this algorithm is assured to converged if $\rho > 0$ is sufficiently small. However (6) will not converge if ρ nears the critical density.

A. Preliminary: Newton's Algorithm and Bifurcations

The OZ equation coupled with any closure relation is an example of a nonlinear integral equation that one cannot solve analytically for most intermolecular potentials. Its solution structure possesses subtleties that depend on the choice of potential and on physical parameters such as density and temperature. Moreover, as those parameters are varied the number of solutions of the equations changes. The mathematical parlance for the parameter value at which such a change is observed is called a *bifurcation point*; this paper is a response to the need for a numerical code that can locate bifurcations or spinodals (which *is* a type of bifurcation) of the OZ-HNC equation in an automated fashion, given that Newton's method alone applied to the OZ equation can locate neither bifurcation points nor spinodals.

Newton's method is designed to solve a very general, possibly high-dimensional equation of the form

$$F(\gamma) = 0, \qquad (8)$$

by taking an initial guess γ_0 and refining through the sequence of iterates defined by

$$\gamma_{n+1} = \gamma_n - dF(\gamma_n)^{-1} F(\gamma_n). \tag{9}$$

In fact this process is commonly used in studies of the OZ equation, but the algorithm requires a fundamental property to hold so that the sequence of iterates (γ_n) can be obtained: at a solution γ^* whereby $F(\gamma^*) = 0$, it must be the case that the matrix of partial derivatives of $F(\gamma)$ at $\gamma = \gamma^*$, denoted $dF(\gamma^*)$, is an *invertible* or *non-singular* matrix (one that has a non-zero determinant). Note that A^{-1} is used here and throughout to denote the inverse of a matrix A.

However, if F is used to represent the OZ equation with HNC closure then Newton's method *will not work* near a candidate spinodal or near the critical region because the matrix $dF(\gamma^*)$ will *always* turn out to be singular in this region. Picard iterations are also commonly used in the literature, but these are just special cases of Newton iterations and so they will not work in these regions.

In order to obtain as much detail of the solution structure as possible, we adopt the pseudo arc-length (PAL) strategy that is due to Keller and others that is now a common tool in bifurcation analysis within the scientific community [7, 10]. Indeed, these techniques have already been used in a density-functional framework, as can be seen in [8] whose authors emphasize the need for the application of bifurcation-based tools in the study of integral equation theories of phase transitions.

Before continuing, we remark that the *continuation method* described in [17] is termed *natural parameter continuation* in the numerical analysis literature and what we propose is quite different. Also, the term *continuation method* is often used for any algorithm that can cope with the presence of bifurcations and other instabilities.

In this paper we explain how one can alter the formulation of Newton's method to locate *spinodals* if they are present, to locate *pseudo-spinodals*, a term that is defined below, and to find the location of pseudo-spinodals as a

function of temperature and density. The algorithms are relatively fast in the sense that they run in Matlab on a single processor Pentium 4(2.6GHz, 2GB RAM) machine with up to 2^{18} mesh points, using the fast-Fourier transform (in the west) FFTw to implement convolution and we use the matrix-free linear solver GMRES that is available as a standard part of the Matlab environment in order to find the Newton updates as defined in (9). To locate a single solution takes of the order of seconds to minutes, depending on the size of the numerical mesh used for the computations.

For illustrative purposes we have presented two scenarios in Figure 1 that would prevent Newton's algorithm from converging when applied to the OZ-HNC equation: one (C_1) is a *branch point, fold bifurcation or pseudo-spinodal* (terms that we consider to be synonymous, although we prefer the term branch point) that is not associated with the divergence of compressibility but is related to a numerical instability because compressibility is large in some sense; and another (C_2) is a *spinodal* along which compressibility does diverge. The former is so named because of the folded geometry of the solution curve near the point BP and this arises because *two* solutions of the equations are present for $0 \leq \rho < \rho_{BP}$.

It is near the label BP that Newton's method would fail because if ρ were just a little less than ρ_{BP}, the fact that two solutions are to be found so close to each other creates a vertical tangent at BP that causes a numerical instability for (9). A similar comment applies to the isothermal solution branch C_2 where the instability arises because of the asymptotically vertical tangent of the graph at the spinodal.

FIG. 1: Schematic of a branch point, fold bifurcation or pseudo-spinodal in C_1 and an isothermal solution branch C_2 with a spinodal.
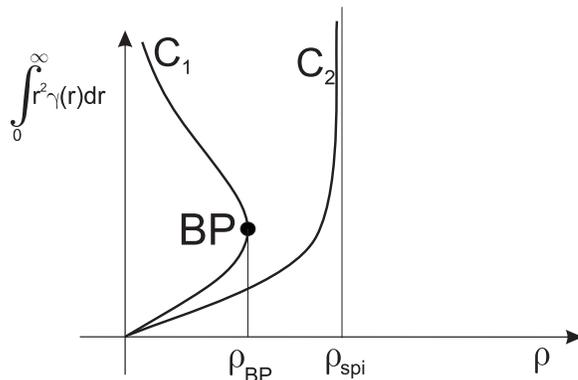
III. LOCATING A SPINODAL: THE PROBLEM

When seeking a spinodal of the OZ-HNC equation, we require solutions that satisfy the condition

$$1 - 4\pi\rho \int_0^\infty r^2 c(r) dr = 0. \tag{10}$$

However, a solution pair (h, c) of (1-2) that satisfies (10) also satisfies $\int_0^\infty r^2 h(r) dr = \infty$ and so can be shown to be associated with an inherent numerical instability.

It therefore seems natural to try and locate a spinodal by obtaining solutions of (1-2) at low density to begin with, which can be done very easily using a Picard iteration for any potential and temperature. Then, by slowly increasing density and holding temperature fixed, one can track the branch of isothermal solutions as closely as possible to a desired spinodal.

However, this approach is doomed to fail if one uses an unmodified Newton method on (1-2) because of the high sensitivity of the solutions to changes in density as one nears the spinodal. One must therefore reduce the incremental changes in density in a fashion that is commensurate with the increases in the integral of h and γ as one nears a branch point or a spinodal.

In [2, 3, 13, 14, 18] the authors have applied a bare Newton method (although sometimes the authors use Picard methods) to study the number of solutions of the OZ equations. While such an approach will be successful away from the critical region, as temperature nears its critical value for, say,

a Lennard-Jones fluid, Newton methods applied to OZ with any closure must cease to converge. Below the critical temperature, a Newton method will also fail unless the values of the density parameter are carefully chosen to ensure that the solution one is seeking is some way away from any spinodal or pseudo-spinodal that may be present.

A. Locating a spinodal: the solution

In order to compute as close to a spinodal as possible we undertake the following operation that is depicted in Figure 2. The procedure begins by treating OZ-HNC (or OZ with any closure) as an equation not just for the correlation function γ but one also considers ρ to be an unknown, but temperature is held at a fixed value.

Thus we have the equation $\gamma = \rho N(\gamma, \beta)$ with two unknowns γ and ρ. We now augment this problem with a new equation and therefore replace equation (6) with the pair

$$G(\gamma, \rho, s) := (\gamma - \rho N(\gamma, \beta), \ \alpha(\gamma, \rho, s)) = (0, 0), \tag{11}$$

where we have added a new unknown s and an auxiliary function α. The function α merely serves as a way of parameterising any solution curve of (6) in (γ, ρ)-space with the auxiliary parameter s that acts as an arc-length variable for this purpose. In [6, 10] one can find the mathematical details of how and why this is done.

There are two points two be made: firstly, by a judicious choice of α we will be able to solve equation (11) for (γ, ρ) as a function of the artificial parameter s; secondly, we shall do this in such a way that equation (11) can be solved *even when one cannot* solve (6) easily using Newton's method for the unknown γ. The reason for this is that Newton's method can fail to find solutions even when they are there; this is not a purely numerical issue but one associated with a change in the solution structure of the underlying equations. Typically, when two solutions are too close together to allow a sufficiently good initial guess to be found then Newton cannot easily proceed as this closeness property

renders the linear system in the Newton iteration numerically ill-conditioned or near-singular. Precisely this situation occurs at a branch point of the OZ-HNC equations.

The point is that when applying a Newton method to (6), the inherent instability of being close to a spinodal forces a numerical instability that renders the linear system within the Newton iteration (given by (9)) a singular linear system. However, one can choose α in such a way that when applying a Newton method to (11), the associated linear system of *that* Newton method *is* non-singular.

FIG. 2: Consider a known solution (γ_1, ρ_1) on a near-spinodal isothermal solution branch C. In order to locate the solution (γ_2, ρ_2), begin by finding the tangent direction of the curve at (γ_1, ρ_1) and use this to locate a suitable nearby initial guess or *linear predictor* (γ_p, ρ_p). Now use (γ_p, ρ_p) as an initial guess for a Newton iteration whose iterates remain in the plane Π and converge to (γ_2, ρ_2); the normal vector of Π is the previously computed tangent direction.
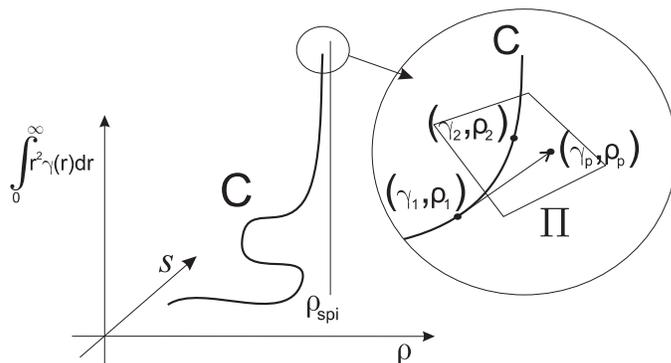

Figure 2 gives a geometric description of this method. Given a solution γ_1 at $\rho = \rho_1$ on a solution curve C, so that $\gamma_1 = \rho_1 N(\gamma_1, \beta)$ and (γ_1, ρ_1) is a vector pair that lies on C, one predicts where a nearby solution on the solution branch will be located by looking a small distance, ds say, along the tangent direction of the curve. This gives an initial guess or *predictor* (γ_p, ρ_p) for a Newton method that is constructed in such a way that the iterates of that method lie within a plane Π whose normal direction coincides with the

11

previously computed tangent direction. This Newton method is iterated to convergence in order to locate (γ_2, ρ_2) and the use of the tangent vector along C automatically adjusts for the fact that the curve *steepens* in the sense that the size of $d\gamma/d\rho$ increases along C near the spinodal.

In order to complete the description of the methodology we have to provide the form of the function α in (11). This we do in the next section.

B. Arc-Length Continuation

As C is a one-dimensional curve we may parameterise it by arc–length s. In principle, there are many possible choices for the function α in (11), but the one used in practise is the linearised or pseudo arc-length constraint given by (again see [10])

$$\alpha(\gamma, \rho, s) = \mathbf{s}_0 \cdot (\gamma - \gamma_0) + \sigma_0(\rho - \rho_0) - (s - s_0),$$

where a dot denotes the inner product of two vectors, as in $(x_1, x_2, .., x_n) \cdot (y_1, y_2, ..., y_n) = \sum_{i=1}^{n} x_i y_i$. Moreover, $(\mathbf{s}_0, \sigma_0)$ is the unit tangent vector at a given point on the solution curve C and we assume the existence of a known solution on C so that $G(\gamma_0, \rho_0, s_0) = 0$, where G is defined in (11).

The full algorithm thus has the following steps, where ds assumes a *fixed, small* value:

(P1) Choose ρ_0 to be sufficiently small that Picard iteration will converge, set $s_0 = 0$ and find $(\gamma_0, \rho_0) \in \mathsf{C}$ using Picard.

(P2) Given a solution $(\gamma_k, \rho_k) \in \mathsf{C}$ at the arc–length parameter s_k, let $s_{k+1} = s_k + ds$ and find the unit tangent vector to C by solving the linear system of equations

$$\partial_\gamma G(\gamma_k, \rho_k, s_k)\overline{\gamma} + \partial_\rho G(\gamma_k, \rho_k, s_k)\overline{\rho} = -\partial_s G(\gamma_k, \rho_k, s_k)$$

for $(\overline{\gamma}, \overline{\rho})$ and then define a *unit* vector $(\mathbf{s}_k, \sigma_k)$ by

$$\mathbf{s}_k = \frac{\overline{\gamma}}{\sqrt{\|\overline{\gamma}\|^2 + \overline{\rho}^2}}, \quad \sigma_k = \frac{\overline{\rho}}{\sqrt{\|\overline{\gamma}\|^2 + \overline{\rho}^2}}.$$

(P3) Apply Newton iteration to $G(\gamma, \rho, s) = 0$ with initial guesses $\gamma = \gamma_k + ds \cdot \mathbf{s}_k$ and $\rho = \rho_k + ds \cdot \sigma_k$ and denote the solution thus found $(\gamma_{k+1}, \rho_{k+1})$.

The algorithm (P1-P3) is still based on Newton's method and both steps (P2) and (P3) require the use of a linear solver and one could use, say, Gaussian elimination (or LU-decomposition) applied to the derivative matrix of (11). However, this would be *extremely* inefficient as it requires the derivative matrix to be constructed and then inverted, so instead we use the *GMRES algorithm*. As is discussed in [12], this is appropriate for integral equations like OZ-HNC and has the particular advantage of never needing to form the derivative matrix of (11) when applying Newton's method within the PAL algorithm.

In practise, ds has to be chosen small enough so that the Newton iteration described in the previous paragraph converges. We altered the value of ds so that if this iteration required a small number of Newton steps then ds would be increased by a fixed factor, reducing ds if the number of iterations were too high; this is especially helpful as the algorithm nears a branch point or spinodal. In practise, we used 0.1 for ds when ρ is small, which decreased to as small as $ds = 10^{-2}$ or 10^{-3} when passing through branch points.

If ds is sufficiently high and two solution branches are to be found sufficiently close together, this may permit the PAL algorithm to *jump* from one solution branch to another; it is this property that initially lead us to finding solution branches of negative compressibility. However, using the Newton-GMRES code detailed in [11, 12] that has also been written in Matlab, we were in fact able to choose temperature and density within the no-solution region and locate such a non-physical solution with little difficulty. This is because the Newton algorithm of [11, 12] (that, note, can be downloaded as the Matlab m-file `oz.m` located at `http://www4.ncsu.edu/~ctk/newtony.html`) always converges to some solution, irrespective of the density that we chose, and this solution was then continued to form an entire isothermal solution branch using the PAL algorithm.

IV.   PSEUDO-SPINODALS

One can exploit one of the properties of matrices that leads to non-convergence of Newton's method (9) in order to track the precise location in the (ρ, β)-plane of where OZ-HNC will possess pseudo spinodals. Now, a matrix A is singular if there is a non-zero vector $\mathbf{k}$ such that $\mathsf{A}\mathbf{k} = \mathbf{0}$ and Newton's method applied to OZ-HNC will fail if the matrix of partial derivatives of $\gamma - \rho N(\gamma, \beta)$ is singular when viewed as a function of γ.

We can apply this idea to (3) as follows: let us find (k, γ, ρ) such that

$$
\begin{pmatrix}
\gamma - \rho N(\gamma, \beta) \\
(I - \rho \partial_\gamma N(\gamma, \beta))k \\
\|k\|^2 - 1
\end{pmatrix}
=
\begin{pmatrix}
0 \\
0 \\
0
\end{pmatrix},
\tag{12}
$$

where A corresponds to the matrix of partial derivatives $I - \rho \partial_\gamma N(\gamma, \beta)$ and I is the identity matrix. The first equation in (12) is a repetition of (3), the second ensures that when Newton's method is applied to (3) it cannot converge: in effect we are using the second equation in (12) to impose the condition that the matrix which is formed from the linearisation of the OZ equation (3) is a matrix the possesses a non-zero null-vector and is therefore a singular matrix. This is precisely the condition that prevents Newton from converging. The third equation in (12) is the condition that k is non-zero, where $\|k\|^2 = \sum_{i=1}^{n} k_i^2$ is used to denote Euclidean distance-squared of the vector $k = (k_1, ..., k_n)$.

One could reformulate (12) as the following equivalent system of equations

$$
\begin{pmatrix}
\gamma - \rho N(\gamma, \beta) \\
\det(I - \rho \partial_\gamma N(\gamma, \beta))
\end{pmatrix}
=
\begin{pmatrix}
0 \\
0
\end{pmatrix},
\tag{13}
$$

where det denotes the determinant of a matrix. However, (13) would not provide for an efficient numerical implementation due to the presence of the determinant.

By solving (12) one obtains the boundary of theoretical convergence of Newton's method applied to (3) in the (ρ, β)-plane which is the locus of branch

points. One can apply either a standard Newton method to (12) with β fixed, or one can use the PAL algorithm in case the approximated curve of branch points has a particularly complicated structure; we have used both approaches in practise.

V. NUMERICAL RESULTS

Before we give the results of our numerical computations, one further remark is in order. When seeking approximate solutions of the OZ-HNC equation, the only element of the problem that requires discretisation is the convolution operator. To achieve this one uses the fact that convolution can be written using the Fourier transform as

$$a * b = \mathcal{H}^{-1}(\mathcal{H}a \cdot \mathcal{H}b), \tag{14}$$

where a, b are two given functions and $\mathcal{H}$ denotes the spherical Hankel transform (the Fourier transform of radially symmetric functions).

It is standard practise in numerical studies of the OZ-HNC equation to truncate the interval of integration in the definition of the Hankel transform to a finite interval $[0, R]$ when solving (1-2). So, given that

$$(\mathcal{H}a)(s) = 4\pi \int_0^\infty \mathrm{sinc}(rs) r^2 a(r) dr$$

and the given inverse transform $(\mathcal{H}^{-1}a)(s) = \frac{1}{8\pi^3}(\mathcal{H}a)(s)$, if we define

$$(\mathcal{H}_R a)(s) = 4\pi \int_0^R \mathrm{sinc}(rs) r^2 a(r) dr$$

and $(\mathcal{H}_R^- a)(s) = \frac{1}{8\pi^3}(\mathcal{H}_R a)(s)$, we can formulate the equation that is to be solved numerically using the PAL algorithm:

$$\begin{aligned}
\gamma &= \rho \mathcal{H}_R^- \left(\mathcal{H}_R(f + e^{-\beta u}(\exp\gamma - 1)) \right. \\
&\quad \times \left. \mathcal{H}_R(f + e^{-\beta u}(\exp\gamma - 1) - \gamma) \right).
\end{aligned} \tag{15}$$

In practise we shall solve (15) approximately, exploiting the FFT in our numerical calculations at every opportunity. One significant difference with our

discretisation (that we do not detail here) and the ones used in all other cited references is the fact that we employ one step of a Richardson extrapolation procedure to obtain $O(n^{-4})$ error estimates for solutions of (15), where n is the numerical mesh size, rather than the $O(n^{-2})$ estimates that are usually obtained. The penalty for this is that while second-order accuracy can be obtain by performing convolution with three FFT operations, our method requires five such operations, but this can be achieved without compromising the $O(n \log(n))$ complexity of the FFT-based numerical convolution algorithm.

A. Computations

The purpose of this section is to illustrate the applicability of the PAL algorithm (P1-P3) to trace solution branches of the OZ-HNC equation with the Lennard-Jones (LJ), Double Yukawa (DY) and Triple Yukawa (TY) potentials, where the Yukawa potentials are chosen to fit the Lennard-Jones potential. For completeness let us define the Lennard-Jones potential

$$u_{LJ}(r) = 4\epsilon((\sigma/r)^{12} - (\sigma/r)^6). \tag{16}$$

The potential well depth ϵ and the particle diameter σ are used to define the thermodynamic quantities in reduced units: $\rho^* = \rho\sigma^3$, $T^* = k_B T/\epsilon = 1/(\epsilon\beta)$. For the numerical calculations we use a numerical mesh size of $n = 2^{12} + 1$ points unless otherwise stated. A relative error tolerance of 10^{-11} in the so-called *maximum vector length* or *norm* [19] was used to measure errors for the Newton iterations that were performed.

Figures 3, 4, 5 and 6

Our first set of computations is best illustrated by comparing Figures 4, 5 and 6, where temperature is held fixed in each computation (at $T^* = 1.6, 1.408$ and 1.3 respectively). We have computed the variation of inverse isothermal compressibility with respect to density, ρ^*, as well as the total correlation functions corresponding to three representative thermodynamic states. As the

temperature decreases the critical temperature of the Lennard-Jones model is approached and this is reflected in values of the inverse compressibility which develops a minimum at a value of ρ^* somewhere between 0.25 and 0.3.

As temperature is reduced further, Figure 6 illustrates the creation of two disconnected solution branches: vapour at low densities and liquid at high densities. Note the W-shaped nature of the vapour isotherm whereby several apparent branch points are present in the region of zero inverse compressibility. This is the reason for the nomenclature *pseudo spinodal* that we have associated with the the branch points as χ^{-1} is typically close to zero when they occur. Figure 6 also shows that one can in fact have an apparently genuine spinodal within the HNC approximation in the sense that the compressibility as it is defined in this paper diverges to infinity. This occurs nonetheless in a manner that corresponds to an unphysical variation of compressibility with respect to changes in density.

The results presented above illustrate the power of the numerical approach desribed in this paper. In previous investigations such as [2, 13] the crossing of inverse compressibility from positive to negative values was not reported. In one of these investigations negative compressibilites were reported but these resulted from a complex-valued solution that itself stems from the existence of a branch point. Figure 6 shows that it is perfectly possible to connect the range of negative values with the positive ones in a continuous fashion along isothermal solution branches of real-valued solutions.

One may ask how two solution branches can appear at low temperatures where only one was present at high temperatures. The answer to this lies in the fact that there *is* another solution branch that exists at the parameter values used in Figure 4, but it is not plotted in this figure for clarity as it only contains solutions of negative compressibility. We have illustrated this phenomenon in Figure 3 where supercritical and subcritical isotherms are labelled (1) and (2) respectively: note that there are *two* supercritical isotherms labeled (1) that have been computed at $T^* = 1.41$, one has positive and one negative compressibility. It may be instructive to compare Figure 3 with [14, FIG.4].

FIG. 3: Four representative isothermal pairs of solution branches where $R = 20\sigma$ and $n = 2^{10} + 1$: the two isotherms labeled (1) are supercritical (both isothermals have been computed with $T^* = 1.41$) whereas the others are for subcritical temperatures.
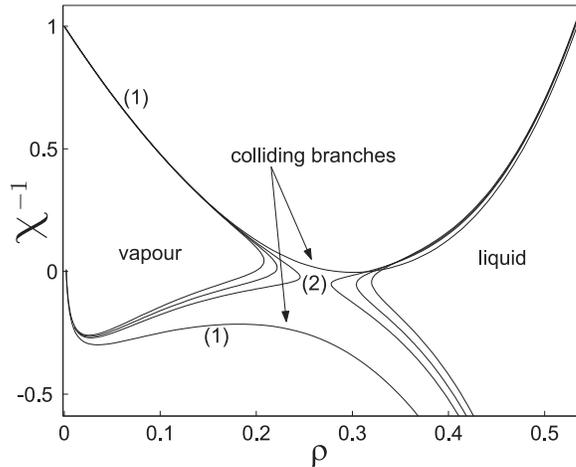

It is very important to realise that the phenomena desribed in this section are associated with solutions of the numerical or computational realisation of the OZ-HNC equations (15) and not necessarily with the OZ-HNC equations themselves; the mathematical reasons for this are explored in detail in [1]. For example, it is easy to see from the convolution theorem applied to OZ that it is **impossible** for a continuous solution of (1) to be realised with zero inverse compressibility, yet it **is** possible to locate continuous solution of (15) with zero inverse compressibility. This comment is central to the design of qualitatively correct discretisation methods for the OZ equation with its various closures, but the analysis that leads to such methods is beyond the scope of this paper.

Figure 7

Although our next computation has a small numerical mesh with only $n = 1025$ points and also has a low cut-off value of $R = 20\sigma$ with $T^* = 1.2$, we have included it to further illustrate the point made in the previous section regarding solutions of negative compressibility. One can see in Figure 7 that we have found many solutions that do indeed have negative compressibility

18

FIG. 4: Inverse isothermal compressibility plotted against density at temperature $T^* = 1.6$ for the Lennard-Jones potential (so that T^* is greater than $T_c^* \simeq 1.4$) where $R = 80\sigma$ and $n = 2^{12} + 1$. Three correlation functions, $r^2 h(r)$, are presented at density values: (a) $\rho^* = 0.1$, (b) $\rho^* = 0.270$ and (c) $\rho^* = 0.55$.
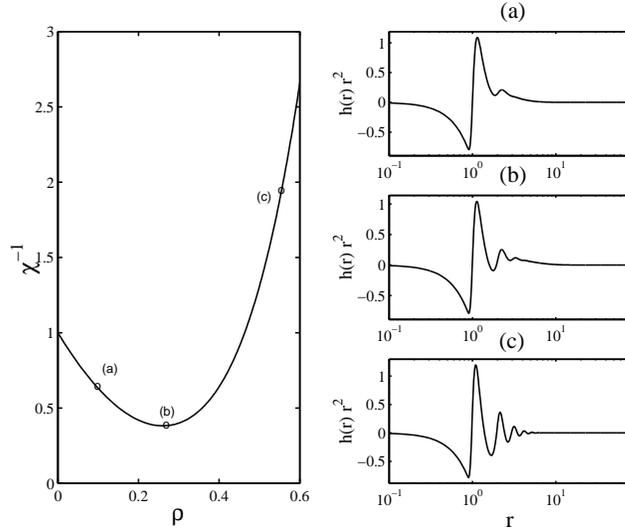

within the so-called no-solution region that are easily located using the PAL algorithm, employing the code from [11] to locate initial points on the branches. The same figure also contains two solution branches of (partially) positive compressibility.

The correlation function $r^2 h(r)$ is indicated in Figure 7(a) at a point on the vapour isotherm before the first branch point and correlation functions computed on other solution isotherms are also shown. Note in particular Figure 7(b) showing the unphysical nature of $r^2 h(r)$ for large values of r.

The vapour solution branch in Figure 7 emanates from the point $(\gamma, \rho) = (0, 0)$ with unit compressibility and this branch extends to higher densities, but it then continues into the region of negative compressibility at around $\rho = 0.12$. It has been reported in the literature that compressibility remains finite in numerical computations when approaching the no-solution region [2, 3, 14, 17, 18], indicating that this region is *not* linked to a phase transition. Our computations indicate that in fact there *are* numerical solutions that have zero

(August 2, 2006)

FIG. 5: Inverse isothermal compressibility plotted against density at temperature $T^* = 1.408$, (T^* just above T_c^*), for the Lennard-Jones potential, $R = 80\sigma$ and $n = 2^{12} + 1$. Three correlation functions, $r^2 h(r)$, are presented at density values: (a) $\rho^* = 0.1$, (b) $\rho^* = 0.270$ and (c) $\rho^* = 0.55$.
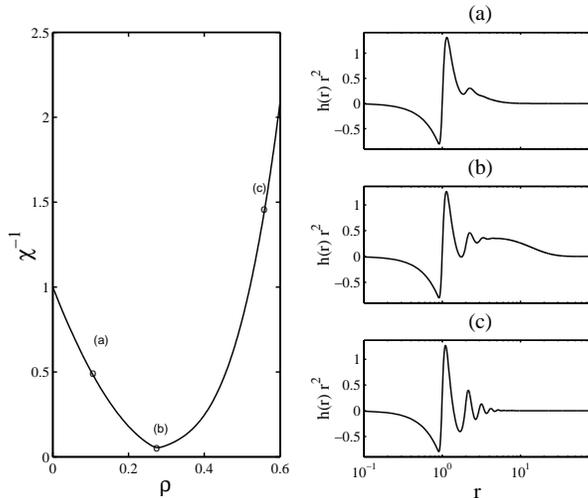
inverse compressibility, but that they occur on isothermal solution branches beyond the first branch point.

Figure 8

Figure 8 illustrates the effect of increasing the cutoff R. In this case we have used $n = 2^{12} + 1$ and $R = 120\sigma$; this plot refines the left-hand branch shown in Figure 7. It is important to note that the increase in accuracy has resolved a number of branch points that were missed when using too coarse a mesh in Figure 7, leading to a W-shaped solution branch with three pseudo spinodals. This is reminiscent of behavior found by Belloni for different potentials [2]. The right hand plots show the total correlation functions of two solutions that are located at the same density either side of a branch point, (a) is a perfectly feasibly physical solution, whereas (b) is not.

Note that we have illustrated solutions that are situated precisely upon the branch point itself in Figure 10 of the next section and in Figure 12 at the end

(August 2, 2006)

FIG. 6: Inverse isothermal compressibility plotted against density at temperature $T^* = 1.3$ (so that $T^* < T_c^*$) for the Lennard-Jones potential with $R = 80\sigma$ and $n = 2^{12} + 1$. Two correlation functions $(r^2 h(r))$ are presented at density values : (a) $\rho^* = 0.1$, (b) $\rho^* = 0.270$ *NO SOLUTION* and (c) $\rho^* = 0.55$.
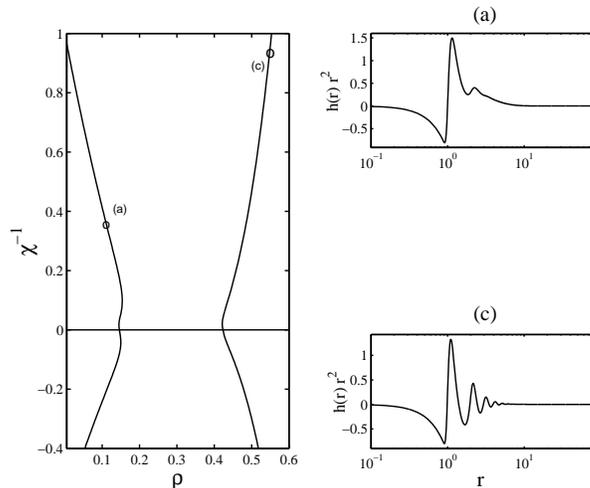

of the paper for computations undertaken for the Yukawa potentials.

Figures 9 and 10

Figure 9(a) shows a computed locus of branch points as defined in section IV, that is, the locus corresponds to the density-temperature pairs for which a branch point is observed and this curve coincides with the one obtained using different algorithms in [13].

While the form of this branch point locus is similar for all of the cut-off values $(R = 20\sigma, 40\sigma, 80\sigma)$ that we chose, the values taken by χ^{-1} along this locus are sensitive to R, as can be seen in Figure 9(b). Each of the curves should, ideally, be very close to zero but they are in fact both above and below zero, depending on the density. The reason for this can be seen in Figures 6 and 7 where the branch point on the vapour branch occurs at positive compressibility before a spinodal is observed, whereas the branch point on the liquid branch occurs at negative compressibility, after an apparent spinodal

(August 2, 2006)

FIG. 7: Inverse isothermal compressibility plotted against density at temperature $T^* = 1.2$ for the Lennard-Jones potential, where $R = 20\sigma$ and $n = 2^{10} + 1$. Three solutions, $r^2 h(r)$, are presented on each curve at: (a) $\rho^* = 0.084$, (b) $\rho^* = 0.419$ and (c) $\rho^* = 0.509$. Solutions for (a) and (c) are clearly seen to lie on the positive χ-part of the vapour and liquid branches.
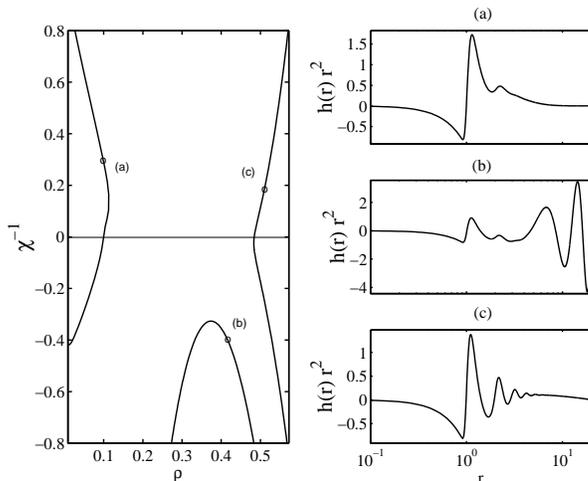
has already been observed.

Examples of the total correlation functions $r^2 h(r)$ computed along the two-parameter parabolic curve from Figure 9 are presented in Figure 10: (A) represents solutions in the vapour region, (B) is at apex from Figure 9(a) and (C) is representative of the liquid region. It is clear in Figure 10(C) that liquid solutions are particulary sensitive to the cut-off value R, although vapour and near-critical solutions are not affected to the same extent.

B. Double Yukawa and Triple Yukawa Potentials

Figures 11 and 12

We also considered the Double Yukawa potential (DY) and Triple Yukawa potentials, respectively (17) and (18) below. The parameters used in (17) taken from [15] are $A_1 = 1.6438\sigma$, $z_1 = 14.7\sigma^{-1}$, $A_2 = 2.03\sigma$ and $z_2 = 2.69\sigma^{-1}$; we

FIG. 8: Inverse isothermal compressibility plotted against density with $T^* = 1.2$ for the Lennard-Jones potential, where $R = 120\sigma$ and $n = 2^{12} + 1$. Two solutions, $r^2 h(r)$, on each curve are presented at: (a) $\rho^* = 0.1127$ and (b) $\rho^* = 0.1122$. Solution (a) located at upper circle in left-hand plot and (b) located at lower circle.
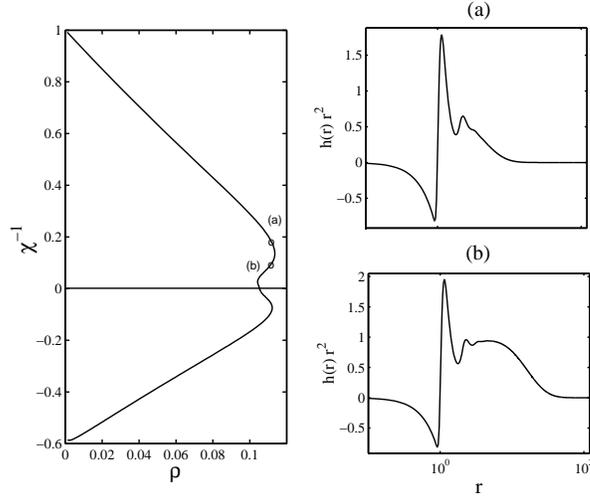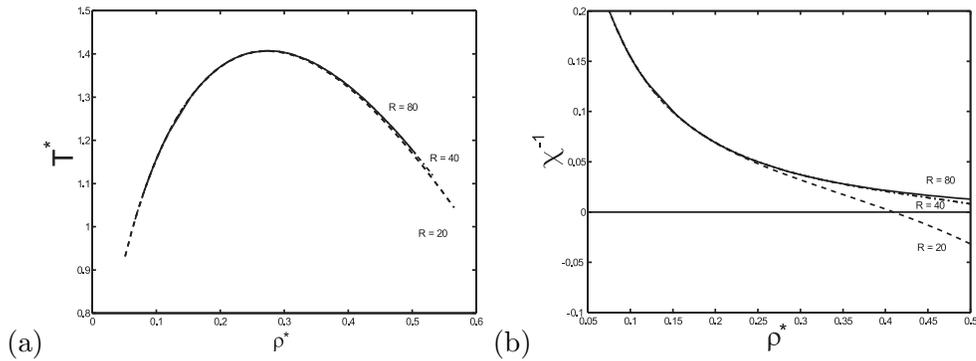

FIG. 9: (a) Locus of branch points and (b) inverse compressibility values for the Lennard-Jones potential for varied cut-off values, R, and $n = 2^{12} + 1$ points. Legend: $R = 80\sigma$ (solid), $R = 40\sigma$ (dash-dot), and $R = 20\sigma$ (dashed line).

recall that $\sigma = 1$ is used throughout. Similarly, the parameters for the Triple Yukawa potential are $c_1 = 2.351\sigma, z_3 = 13.446\sigma^{-1}, c_2 = 0.910, z_4 = 3.482\sigma^{-1}$ and $z_5 = 1.317\sigma^{-1}$ in (18). In contrast to the Lennard–Jones potential which has algebraic decay, the double–Yukawa and triple Yukawa potentials decay

(August 2, 2006)

FIG. 10: Distribution functions $r^2h(r)$ at locations along the branch point locus from Figure 9 for cut-off values $R = 20\sigma, 40\sigma$ and 80σ, using $n = 2^{12} + 1$ points and the Lennard-Jones potential: $(\rho^*, T^*) = (0.122,1.23)$ (A), $(0.275,1.407)$ (B), and (C) $(0.503,1.170)$. Note that (B) represents solutions at the critical apex of the locus of branch points from Figure 9.
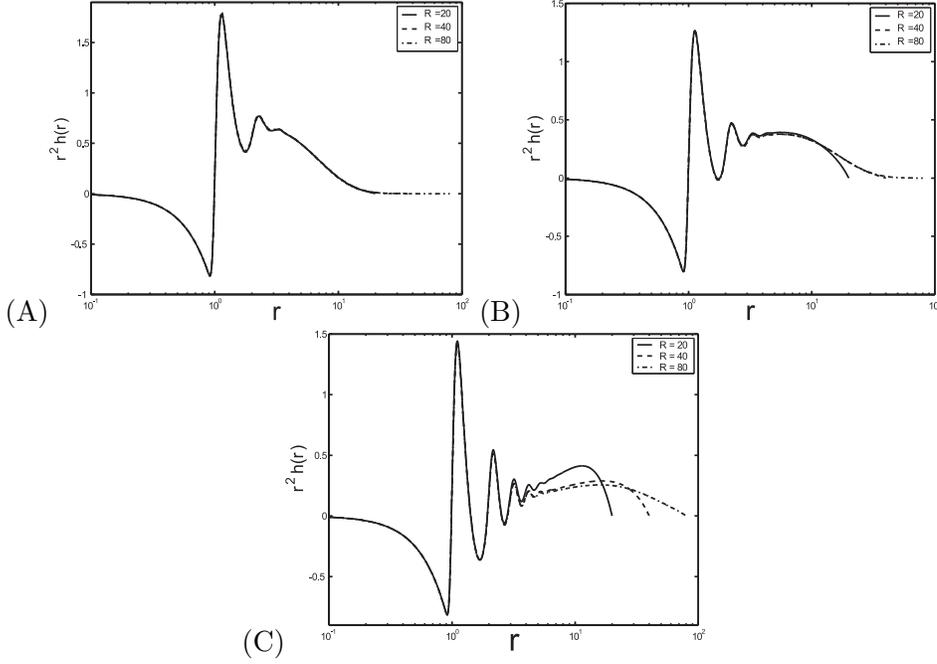
exponentially and are given as follows:

$$u_{DY}(r) = \frac{\epsilon}{r}\left(A_1 e^{-z_1(r-\sigma)} - A_2 e^{-z_2(r-\sigma)}\right) \qquad (17)$$

and

$$u_{TY}(r) = \frac{c_1\epsilon}{r}\left(e^{-z_3(r-\sigma)} - c_2 e^{-z_4(r-\sigma)}\right.$$
$$\left. -(1-c_2)e^{-z_5(r-\sigma)}\right). \qquad (18)$$

The purpose of these computations is to compare the loci of branch points of all three potentials and to investigate whether it is the relatively slow decay of the tail of the Lennard-Jones potential that is responsible for the large values taken by χ^{-1} along this loci as shown in Figure 9.

The reason for doing this is that this figure gives a measure of how close a branch point or pseudo-spinodal is to representing a true spinodal. As can be

FIG. 11: (a)Locus of branch points for the (A) Lennard-Jones (B) Double Yukawa and (C) Triple Yukawa potentials for cut-off value $R = 80\sigma$ and $n = 2^{12} + 1$ points. (b) Inverse compressibility values along the above locus of branch points for LJ, DY and TY potentials.
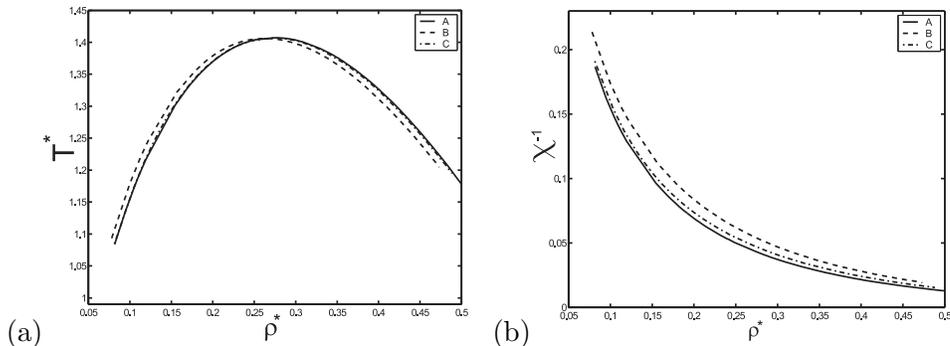

seen in Figure 11(b), the loci of values taken by χ^{-1} are qualitatively similar for all three potentials, as is the form of the branch point locus shown in Figure 11(a). We therefore conclude that it is not the slow decay of the tail of the Lennard-Jones potential that leads to the poor approximation of spinodals by branch points. For further comparison with the Lennard-Jones case, we have included Figure 12 which plots the total correlation functions taken from vapour, critical and liquid regions of the branch point curve Figure 11(a) for both double and triple Yukawa potentials.

VI.   CONCLUSIONS

We have introduced an automated numerical methodology to solve the Ornstein-Zernike equation at different temperatures and densities and have focused on the HNC closure relation and the Lennard-Jones potential as a case study. We have shown that by employing the pseudo arc-length continuation method one can compute solutions that are not possible to find when applying Newton or Picard methods directly. Moreover, our approach confirms previous analyses of the OZ-HNC equation that have suggested the existence

25

FIG. 12: Plots of $r^2h(r)$ at various locations along the two-parameter branch point locus from Figure 11 for the DY(a) and TY(b) potentials: $(\rho^*, T^*)= (0.122, 1.23)$ (A), (0.275, 1.407) (B) and (0.480, 1.210) (C). Label (B) represents solutions at the apex of the branch point locus from Figure 11(a).

(a)   (b)
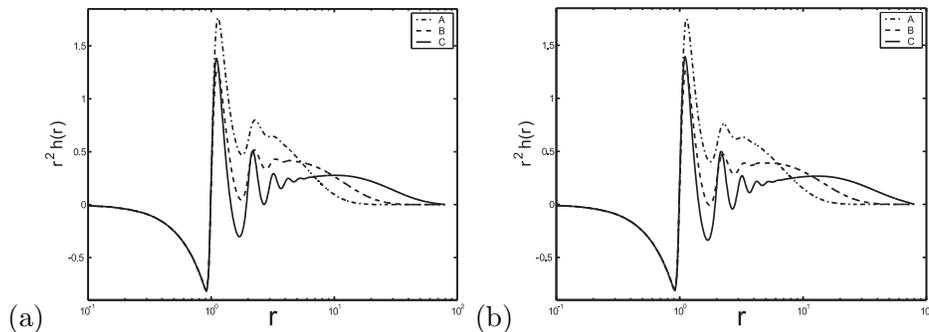
of square root branch points separating physical and unphysical solutions.

One advantage of PAL continuation is that it can pass through branch points in a continuous fashion which represents the main improvement over previous approaches. Interestingly, we have found real solutions within the so-called no solution region. However, the solutions do not connect with the branch points and have negative compressibility and are therefore unphysical.

Moreover, we have been able to compute solutions of zero inverse compressibility on both liquid and vapour branches for potentials with an attractive tail, provided that temperature is sufficiently low. The vapour solution branch shows W and S-shaped structures at low temperature with as many as three solutions for a given density each with positive compressibility, provided that the cut-off parameter R used in the discretisation of (15) is sufficiently large.

[1] R. E. Beardmore, A. T. Peplow, and F. Bresme. A numerical bifurcation analysis of the Ornstein-Zernike equation with hypernetted chain closure. Submitted to SIAM J. Sci. Comput., see `http://www.ma.ic.ac.uk/~rebear`, January

2006.

[2] L. Belloni. Inability of the hypernetted chain integral equation to exhibit a spinodal line. *J. Chem. Phys.*, 98(10), 1993.

[3] J.J. Brey and A. Santos. Absence of criticality in the hypernetted chain equation for a truncated potential. *Mol. Phys.*, 57:149–160, 1986.

[4] P. T. Cummings and P. A. Monson. Solution Of The Ornstein-Zernike Equation In The Vicinity Of The Critical-Point Of A Simple Fluid. *J. Chem. Phys*, 82:4303–4311, 1985.

[5] P. T. Cummings and G. Stell. Critical-Behavior Of The Yukawa Fluid In The Mean Spherical Approximation. *J. Chem. Phys*, 78:1917–1923, 1983.

[6] E. J. Doedel. Lecture notes on numerical analysis of bifurcation problems. Hamburg, can be downloaded from `http://www.cds.caltech.edu/ hinke/courses/CDS280/`, 1997.

[7] E. J. Doedel, R.C. Paffenroth, A.R. Champneys, T.F. Fairgrieve, Yu.A. Kuznetsov, B. Sandstede, and X. Wang. Auto 2000: Continuation and bifurcation software for ordinary differential equations (with homcont). Technical Report, Caltech; see also `http://indy.cs.concordia.ca/auto/`, 2001.

[8] L. J. D. Frink and A. G. Salinger. Rapid analysis of phase behavior with density functional theory. II. capillary condensation in disordered porous media. *J. of Chemical Physics*, 118(16):7466 – 7476, 2003.

[9] J.P. Hansen and I.R. Macdonald. *Theory of Simple Liquids*. Academic Press, London, 1976.

[10] H. B. Keller. *Numerical Solution of Bifurcation and Nonlinear Eigenvalue Problems*. Academic Press, New York, ed. P. Rabinowitz, 1977.

[11] C. T. Kelley. *Solving Nonlinear Equations with Newtons Method*. SIAM, Philadelphia, 2003.

[12] C. T. Kelley and B. Mongomery-Pettitt. A fast solver for the Ornstein - Zernike equations. *J. Comp. Phys.*, 197:491 – 501, 2004.

[13] E. Lomba and J.L. Lopez-Martin. On the solutions of the hypernetted-chain equation inside the gas-liquid coexistence region. *J. Stat. Phys.*, 80(825), 1995.

[14] P. D. Poll and N. W. Ashcroft. Critical behaviour of the hypernetted chain equation. *Phys. Rev. A*, 35(12):5167–5173, 1987.

[15] Elisabeth Scholl-Paschinger. *Phase Behaviour of Simple Fluids and their Mixtures*. PhD thesis, Intitut fur Theoretische Physik, Vienna, February 2002.

[16] C. A. Stuart and G. Vuillaume. A discretised nonlinear eigenvalue problem with many spurious branches of solutions. *Zeitschrift für Analysis und ihre Anwendungen (ZAA)*, 20(1):183–192, 2001.

[17] D. A. Tikhonov and G. N. Sarkisov. Singularities of solutions of the Ornstein-Zernike equation within a gas-liquid transition region. *Russian J. Phys. Chem.*, 74(3), 2000.

[18] R. O. Watts. Hypernetted-Chain Approximation Applied to a Modified Lennard-Jones Fluid. *J. Chem. Phys.*, 50(1358), 1969.

[19] If $\mathbf{x} = (x_1, x_2, ..., x_n)$ then the maximum vector length or norm is $\|\mathbf{x}\|_{\mathsf{max}} = \max_{1 \le i \le n} |x_i|$.